NeuroImage 165 (2018) 158–169

Contents lists available at ScienceDirect

NeuroImage

journal homepage: www.elsevier.com/locate/neuroimage

Combining region- and network-level brain-behavior relationships in a structural equation model

Taylor Bolt [a,*], Emily B. Prince [a], Jason S. Nomi [a], Daniel Messinger [a], Maria M. Llabre [a], Lucina Q. Uddin [a,b]

[a] Department of Psychology, University of Miami, Coral Gables, FL, USA
[b] Neuroscience Program, University of Miami Miller School of Medicine, Miami, FL 33136, USA

A B S T R A C T

Brain-behavior associations in fMRI studies are typically restricted to a single level of analysis: either a circumscribed brain region-of-interest (ROI) or a larger network of brain regions. However, this common practice may not always account for the interdependencies among ROIs of the same network or potentially unique information at the ROI-level, respectively. To account for both sources of information, we combined measurement and structural components of structural equation modeling (SEM) approaches to empirically derive networks from ROI activity, and to assess the association of both individual ROIs and their respective whole-brain activation networks with task performance using three large task-fMRI datasets and two separate brain parcellation schemes. The results for working memory and relational tasks revealed that well-known ROI-performance associations are either non-significant or reversed when accounting for the ROI's common association with its corresponding network, and that the network as a whole is instead robustly associated with task performance. The results for the arithmetic task revealed that in certain cases, an ROI can be robustly associated with task performance, even when accounting for its associated network. The SEM framework described in this study provides researchers additional flexibility in testing brain-behavior relationships, as well as a principled way to combine ROI- and network-levels of analysis.

Introduction

Large publicly available datasets and a wide array of analytic techniques provide a wealth of fMRI data for cognitive neuroscientists interested in exploring individual differences. However, the proliferation of analytic approaches makes the principled selection of one approach over another challenging. Criticism of fMRI brain-behavior association studies, particularly region-of-interest (ROI) based analyses (Vul et al., 2009; Yarkoni, 2009; Yarkoni and Braver, 2010), highlight the potential for misleading conclusions without a methodologically informed approach. One often-overlooked issue in discussions of fMRI brain-behavior associations is the choice of the *level of analysis* of the 'brain' variable (independent variable, IV) that is correlated with the 'behavioral' variable (dependent variable, DV).

The level of analysis of fMRI data can extend from a single voxel, to a brain region, to a network comprised of multiple brain regions, to all voxels in the brain. Most studies to date have used blood-oxygen-level dependent (BOLD) activation estimates at the level of an ROI, a region *hypothesized* to be of relevance to the behavioral variable, as the brain variable (e.g. Grabner et al., 2007; Hampson et al., 2006; Hubbard et al., 2005; Molenberghs et al., 2016; Rypma & D'Esposito, 1999; Stephan et al., 2003; Todd and Marois, 2005; Vossel et al., 2016). However, as observed in both resting-state and task-based activation studies, brain regions do not function in isolation, but as parts of larger collections of interacting brain regions that form networks (Bullmore and Sporns, 2009; Calhoun et al., 2008; Damoiseaux et al., 2006; Fox et al., 2005; Smith et al., 2009). Thus, several recent studies have used network-level brain variables to examine brain-behavior associations (Fornito et al., 2012; Krmpotich et al., 2013; Leech et al., 2011; Mišić and Sporns, 2016; Nelson et al., 2016). In this study, we attempt to bridge ROI- and network-level BOLD activation estimates in a novel brain-behavior analysis approach. We offer a simple structural equation modeling (SEM) framework to formulate and test hypotheses regarding both region- *and* network-level brain-behavior associations simultaneously.

Properties of the functional organization of the human brain suggest that analysis at both levels would be fruitful. Resting-state fMRI studies have discovered a hierarchical functional organization of the human brain (Bassett et al., 2008; Doucet et al., 2011; Ferrarini et al., 2009; Meunier et al., 2010), in which smaller communities of brain regions are nested within larger communities of brain regions, and so on. In addition, this observed hierarchical structure has been associated with subject-level behavioral variables. Suk et al. (2016) used a state-space model with a deep learning algorithm for detecting hierarchical relationships among ROIs to classify mild cognitive impairment patients versus healthy

* Corresponding author.
E-mail address: tsb46@miami.edu (T. Bolt).

https://doi.org/10.1016/j.neuroimage.2017.10.007
Received 28 March 2017; Received in revised form 3 October 2017; Accepted 5 October 2017
Available online 10 October 2017

controls with greater accuracy than other conventional approaches. Incorporating this observed hierarchical structure explicitly into an approach for examining brain-behavior associations with activation estimates from task fMRI would be beneficial. Examination of both levels of analysis can assist in determining whether neural activation at the ROI- or network-level is most relevant for a given behavior. For example, it is possible that 'coarse' network-level activation is more associated with general attention performance in a visually-guided attention task, but activation within a specialized ROI may be associated with performance on a task requiring attention to human facial features specifically.

In a traditional ROI-based brain-behavior analysis, estimates derived from a single ROI for each individual, such as BOLD activation during a task block of interest, are correlated with a behavioral variable of interest collected during the scan (e.g. task performance measures, such as accuracy) or outside of the scanner (e.g. intelligence, age, or disease severity). The inference that the ROI in question is uniquely associated with the behavioral variable is contingent upon the assumption that other relevant variables associated with either the ROI or behavioral variable were taken into account; otherwise, an omitted-variable bias may occur (Clarke, 2005). Importantly, the collinearity between the ROI and the network of which it is a member should be considered when estimating the ROI's association with a behavioral variable. In a network-level brain-behavior association study, network-level estimates derived from multivariate techniques (e.g. independent components analysis or graph-theoretical techniques) are correlated with a behavioral variable, with potential unique associations between the constituent ROIs of the network and the behavioral indicator ignored. In order to capture both of these levels of analysis we propose a novel brain-behavior analysis in the form of an SEM model that incorporates insights from both levels of analysis (ROI- and network level).

SEM has previously been used in fMRI to test hypothesized models of associations among ROIs (Beaty et al., 2016; de Marco et al., 2009; Gates et al., 2011; James et al., 2009; Karunanayaka et al., 2014; Kim et al., 2007; Schlösser et al., 2006; Sturgeon et al., 2014; Zhuang et al., 2005). For example, Kim et al. (2007) proposed a two-stage unified SEM plus general linear model (GLM) approach for analyzing ROI functional connectivity, incorporating both an SEM estimation stage for estimating ROI-ROI path estimates, and a GLM stage that predicts the estimated path coefficients from subject-level covariates (e.g. intelligence, age, gender, etc.). Another related approach is dynamic causal modeling (DCM; Friston et al., 2003), where the ROI-ROI path estimates are estimated by the modulating effect of external inputs on state variables, which included neuronal activity and other biophysical factors. These path analysis models between observed ROIs represent a special case of SEM. However, *latent* multivariate modeling features of the SEM approach are rarely incorporated into fMRI analysis. In this study, we describe a structural regression model incorporating network- and ROI-level brain-behavior associations into a latent variable model. This framework can be divided into two steps: a measurement component specifying all constituent ROIs of an activation network as indicators of a latent variable representing the larger network, and a structural model separately estimating the association of the hypothesized ROI and activation network variable with a behavioral indicator. This framework allows the researcher to estimate the unique association between ROI activation and a behavioral indicator, by removing the separate association between the overall network activation and the behavioral indicator.

We illustrate this approach using a large neuroimaging dataset provided through the Human Connectome Project (HCP; Barch et al., 2013). We applied the framework to three task datasets from the HCP that were observed to have sufficient variability in task performance across participants: an N-back working memory task, a relational processing task, and an auditory arithmetic task. In order to predict brain-behavior relationships, we chose tasks that had less than 100% accuracy for the majority of participants. Behavioral performance in the working memory task, relational task, and arithmetic task has traditionally been associated with activation in the dorsolateral prefrontal cortex (DLPFC; Barbey et al., 2013; Barch et al., 1997; Owen et al., 2005; Rypma & D'Esposito, 1999), rostrolateral prefrontal cortex (RLPFC; Bunge et al., 2009; Christoff et al., 2001), and bilateral temporo-parietal junction (TPJ; Ansari, 2008; Butterworth and Walsh, 2011; Grabner et al., 2007, 2007), respectively. However, to our knowledge, studies to date have only considered these regions (or a small subset of regions) in isolation when determining the association between task-activation estimates in these brain areas and behavioral performance. This may be problematic, as the DLPFC and RLPFC are considered components of a larger fronto-parietal network (FPN), consisting of regions in the lateral prefrontal and posterior parietal cortex (Cole et al., 2013; Power et al., 2011; Zanto and Gazzaley, 2013). Additionally, the TPJ is often considered as a component of the salience/cingulo-opercular network (S/CO), consisting of the dorsal anterior cingulate cortex, anterior insular cortex, and inferior parietal cortices (Gordon et al., 2016; Power et al., 2011). This raises the possibility that the entire FPN or S/CO network, rather than an individual network ROI, is a better predictor of task performance. To test this, we simultaneously estimated the unique association between ROI (located in the DLPFC, RLPFC, and TPJ) activation and task accuracy while accounting for the relationship between overall FPN and S/CO network activation within the SEM framework outlined above.

Methods and materials

Participants

Neuroimaging data from 207 non-twin, healthy, right-handed adults (Mean age = 28.61 years (SD: 3.85, range: 22–36); 103 female) made available through the HCP-2014 500 subject release were used for this study. Participants were recruited from the area surrounding Washington University (St. Louis, MO). All participants gave informed consent before participating in the study, as described in Van Essen et al. (2013). Out of the 207 total participants, 200 completed the working memory task, 197 completed the relational task, and 196 completed the auditory arithmetic task. Data were collected over the course of several visits to the scanner and made available to the public as a complete dataset.

Task descriptions

Complete task descriptions have been published by Barch et al. (2013). All three tasks involved two alternating blocks of active and control conditions. The active condition was designed to differ only from the control condition with respect to the cognitive process of interest (working memory for the working memory task, relational processing for the relational task, arithmetic processing for the auditory task) so that particular process is isolated from possible confounding processes, an approach known as cognitive subtraction (Sternberg, 1969). The behavioral variable of interest for each task was average accuracy (percentage of correct responses) during the condition of interest rather than average reaction time, which did not differentiate between correct and incorrect responses.

The working memory task was an N-Back task, a popular measure of working memory which involves monitoring and in-time updating of remembered information (Owen et al., 2005). The task consisted of two runs of 0-back and 2-back blocks with faces, places, tools, and body parts presented as stimuli. For each of the two runs, the four stimulus types were presented in separate blocks. Half of the blocks within each run consisted of a 2-back working memory task (active condition), where participants indicated (through a press on a button box) whether the current stimulus presentation was the same as the stimulus two presentations back. The other half of the blocks within each run consisted of a 0-back working memory task (control condition), where participants indicated (through a press on a button box) whether the current stimulus matched a target cue presented at the start of each block. The behavioral variable of interest from this task was accuracy (percentage of correct

responses) on 2-back trials.

For the relational task, participants were presented with pairs of objects and told to distinguish them on participant or experimenter-specified dimensions. The stimuli were six different shapes, each filled with one of six textures. In the participant-specified blocks (active condition), participants were presented with two pairs of objects (one pair at the top of the screen, and the other pair at the bottom). Participants decided what dimension differed across the top pair: shape or texture. They then decided whether the bottom pair differed along that same dimension. In the experimenter-specified blocks (control condition), participants still saw the pair of objects on the top of the screen, but only one object on the bottom. They also saw either the word "shape" or "texture" in the middle of the screen and were asked to decide whether the bottom object matched the top pair along that dimension. As with the working memory task, the behavioral variable of interest from this task was accuracy (percentage of correct responses) across all participant-specified trials.

For the arithmetic task, participants were presented with interleaved blocks of arithmetic and story conditions. While the original development of this task was intended to study language processing, with the story condition as an active condition and the arithmetic condition as a control condition, the contrast was reversed to study arithmetic processing. In the story condition (control condition), participants were presented with brief auditory stories, followed by a 2-alternative forced-choice question that asked participants about the topic of the story. In the arithmetic condition (active condition), participants were aurally presented addition and subtraction problems (with varying degrees of difficulty), followed by a 2-alternative forced choice question for the correct answer to the problem. To control for differences in numerical ability across participants, the arithmetic condition was adaptive and maintained a similar level of difficulty across participants. As with the working memory task and relational task, the behavioral variable of interest from this task was accuracy (percentage of correct responses) across all arithmetic trials.

Task fMRI acquisition and preprocessing

Acquisition and preprocessing procedures for the HCP pipeline have been described in previous publications (Barch et al., 2013; Glasser et al., 2013; Van Essen et al., 2013). Additional details about the acquisition and preprocessing procedures are included in the *Supplementary Materials*.

ROI activation estimates

The brain variable of interest in the SEM analysis was participant-level ROI activation estimates from subtraction contrasts for all three tasks. The subtraction contrast represents the degree of voxel activation/de-activation in the active condition relative to the control condition. We used two independent whole-brain parcellation schemes for ROI selection and for specification of network membership to ensure the results were not contingent upon a particular parcellation scheme. This was an important reliability check to ensure that the results are robust across various parcellations and network definitions. The 264 ROI parcellation provided by Power et al. (2011) and the 333 ROI parcellation provided by Gordon et al. (2016) are referred to in the main text as the 'Power' and 'Gordon' parcellation, respectively. We decided to use an *a priori* established parcellation of nodes for two reasons: 1) we wanted to test our analyses on regions that have previously been found to be correlated with the cognitive process of interest, as opposed to defining these nodes from task-activation patterns, and 2) we wanted to avoid the dangers of 'double dipping' by defining our nodes from activation estimates in the task and then using the same ROI activation estimates for a brain-behavior correlation (spurious correlations could result if variance of the activation estimates is related to the accuracy scores; (Kriegeskorte et al., 2009)). The Power et al. (2011) parcellation is a collection of 264 spherical ROIs derived from meta-analytic task activation coordinates and volume-based resting-state functional connectivity data. The Gordon et al. (2016) parcellation is a collection of cortical gray-matter ROIs derived from a boundary mapping technique applied to surface-based resting-state functional connectivity data. For each participant, subtraction-contrast estimates for all 264 ROIs (6 mm spheres) from the Power parcellation and 333 ROIs from the Gordon parcellation (transformed into volume space) were computed by averaging all voxel standardized estimates (i.e. participant-level subtraction contrasts) contained in each ROI.

We chose one ROI from each parcellation scheme (Fig. 1) for all three tasks located in brain regions previously implicated in performance of that particular task. These ROIs were chosen to determine if activation estimates from ROIs previously implicated in performance of each task significantly predict task performance above and beyond the association between task performance and the entire network's activation estimates. Note that each single ROI selected was a member of the larger network. For the working memory task, an ROI in the right DLPFC was chosen from each parcellation (Barbey et al., 2013; Owen et al., 2005; Rypma & D'Esposito, 1999). For the relational task, an ROI in the left RLFPC was chosen from each parcellation (Badgaiyan et al., 2002; Bunge et al., 2009; Christoff et al., 2001). Both ROIs are components of the larger FPN consisting of 23 and 24 other ROIs in the Power et al. (2011) and Gordon et al. (2016) parcellations, respectively. For the auditory arithmetic task, an ROI in the right TPJ was chosen from each parcellation (Ansari, 2008; Butterworth and Walsh, 2011; Grabner et al., 2007, 2007; Price et al., 2013). Previous studies have implicated both the right and left TPJ in numerical cognition, but in the current data we chose the right TPJ, as the ROIs from both parcellations in the left TPJ were not significantly ($p > 0.05$) associated with task performance in the arithmetic task. The right TPJ was a component of the salience network in the Power et al. (2011) parcellation, consisting of 18 other ROIs, and a component of the cingulo-opercular network in the Gordon et al. (2016) parcellation, consisting of 40 other ROIs. Despite different labels, each network had significant overlap in the spatial coordinates of each ROI (Fig. 1).

As we describe further in the *Discussion*, the choice of the hypothesized ROI and the network parcellation are important decisions that must be given serious consideration. This issue is not unique to the SEM approach, but to all ROI-based analyses, such as seed-based functional connectivity analyses (Cole et al., 2010) and activation-based ROI selection (Poldrack, 2007). In fact, parameters provided for the measurement model discussed below provide ways of testing for the adequacy of the choice of network parcellation and hypothesized ROI. For example, overall model fit statistics of the measurement model provide objective criteria for determining which network parcellations are most appropriate for modeling the dependencies among ROIs within the network of interest (e.g. FPN).

Structural equation modeling framework

As outlined above, the SEM framework for estimating ROI- and network-level activation associations between behavioral performance in the task proceeded in two steps: a measurement component and a structural component. The measurement component consisted of a confirmatory factor analysis (CFA) and the structural component consisted of a path analysis that specified causal relationships between the components of the measurement model and the behavioral indicator. These types of SEM models are commonly referred to as structural regression models. For the measurement component, each ROI in the network was modeled as a linear function of latent network activation plus ROI-specific activation combined with random error. Explicitly, the measurement model represents the BOLD activation estimate of each individual for an ROI in the network as a linear combination of network-level activation (i.e. common factor) and ROI-specific activation (i.e. specific factor plus random error):

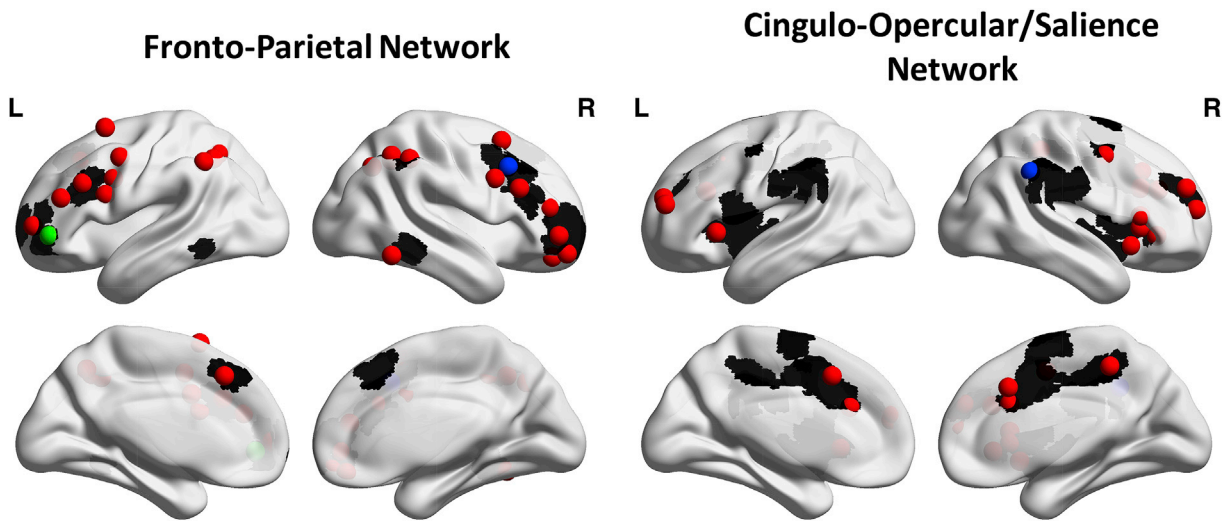

Fig. 1. Brain Regions of Interest in FPN and CO/S Network of Both Parcellations. Visualization of hypothesized ROIs and associated networks, the FPN and CO/S networks, on a surface brain template (Xia et al., 2013). Power parcellation ROIs are displayed as spherical ROIs, and the Gordon ROIs are displayed as surface drawings (black). Hypothesized spherical Power ROIs are distinguished from other spherical network ROIs by color (FPN: right DLPFC – blue, left RLPFC – green; CO/S: right TPJ – blue), and associated Gordon ROIs are the surface regions that overlap with the hypothesized spherical ROIs.

$$X_{i,j} = \lambda_j \theta_i + \delta_{i,j} \quad (1)$$

where $X_{i,j}$ is the ROI activation estimate of the *jth* ROI for the *ith* individual, λ_j is the factor loading describing the association between the *jth* ROI and the network, θ_i is the latent network activation for the *ith* individual, and $\delta_{i,j}$ is the ROI activation estimate of the *jth* ROI for the *ith* individual unrelated to its activation due to the latent network.

In the structural component, associations between the network latent variable and task performance, and between the chosen ROI and task performance were estimated, specified by paths proceeding from the network latent variable and hypothesized ROI variable to the behavioral variable. These two parameter estimates represented the association between network activation estimates and task performance, and the association between the unique ROI activation estimates and task performance, respectively. Explicitly, the structural model predicting task performance from the network activation estimates and the unique ROI activation estimates can be represented as:

$$Y_i = \beta_1 \theta_i + \beta_2 X_i + \varepsilon_i \quad (2)$$

where Y_i is the task performance score for the *ith* individual, β_1 is the beta weight relating the latent network activation estimate to task performance scores, θ_i is the latent network activation for the *ith* individual, β_2 is the beta weight relating the ROI network activation estimate to task performance scores, X_i is the ROI activation estimate for the *ith* individual, and ε is the disturbance for the *ith* individual.

Measurement model (Eq. (1))

The measurement model results provided an estimate of network activation and unique ROI-specific activation. To fix the scale of the latent variable, there are two commonly used approaches: 1) constrain a chosen ROI-network factor loading to 1, or 2) constrain the variance of the latent variable to 1. We chose the latter, as there was no *a priori* indication of the most representative ROI of the network.

The adequacy of the hypothesized measurement model is assessed using the magnitude of the network-ROI factor loadings and global fit indices (Bentler, 2007; Fan et al., 1999; Iacobucci, 2010). Network-ROI factor loadings (λ in Eq. (1)) represent the association between across-subject activation estimates of the ROI and the latent network variable. Standardized network-ROI factor loadings typically vary from −1 to 1, with larger values representing stronger negative and positive associations, respectively. In some cases, factor loadings can exceed 1 in absolute value when there is multicollinearity among the observed variables (i.e. ROIs) that load on the factor. Constituent ROIs are expected to have moderate to strong network-ROI factor loadings, as network models assume that constituent ROIs of a network exhibit synchronous signal dynamics. For this study, a conservative network-ROI factor loading threshold was used ($\lambda > 0.5$), such that ROIs with network-ROI factor loadings below this threshold were removed from the network. This was to check that the original ROI-network assignments of the Gordon and Power parcellation were reflected in our data, and that adequate model fit was obtained. Importantly, the choice of factor-loading cut-off did not change the results of our analysis of the structural model (S2 Table). Recommendations for factor-loading cut-offs vary between researchers from as low as $\lambda > 0.3$ to as high as $\lambda > 0.7$ (Comrey and Lee, 1992; Hair et al., 2013; MacCallum et al., 1999; Peterson, 2000). We recommend that researchers consider the following when choosing factor loading cut-offs: 1) the choice of factor-loading cut-off should be driven primarily to achieve acceptable levels of overall fit for the measurement model, as opposed to simply picking and choosing ROIs of interest, and 2) the researcher should demonstrate that whatever cut-off is used to achieve adequate levels of overall model fit, that this cut-off does *not* change the main results of the analysis (as noted above, the chosen cut-off used above does not affect the results of our analysis).

In every measurement model fitted below, several ROIs were allowed to covary to achieve adequate overall levels of model fit. Covariances among ROIs were allowed to covary in a data-driven manner by using the modification indices provided by Mplus with the default critical value of 10 (i.e. chi-square change larger than 10 if the parameter is added to the model). These modification indices are provided by Mplus for the original model (with no covariance parameters) to guide modification of the model to achieve higher levels of overall fit. Importantly, the structural path estimates between the network/ROI and the behavioral indicator were identical between the covariance-free and covariance-added model, indicating that the network/ROI and behavioral variable relationships in this study were robust to changes in this aspect of the measurement model.

Structural model (Eq. (2))

The structural model estimated the overall network and ROI association with task performance. Importantly, while the measurement model was first considered separately, the final model included both

measurement model and task performance components estimated simultaneously. Both the measurement and final model (including structural components) were estimated with a *Robust Maximum Likelihood* (MLR) estimator as implemented in Mplus software (Muthén and Muthén, 2011). The MLR estimates values of the structural regression model that maximize the likelihood between the estimated covariance matrix and the observed covariance matrix. The observed covariance matrix represents the observed unstandardized correlation between the activation estimates for each pair of ROIs, the estimated covariance matrix represents the unstandardized correlation between each pair of ROIs implied by the model. The proposed model is illustrated by a path diagram in Fig. 2. Example code for running this analysis in Mplus is provided in the supplementary materials (S3 Example Code).

Four global fit indices were used to compared the overall fit of each model to the data: root mean square error of approximation (RMSEA), comparative fit index (CFI), Tucker-Lewis index (TLI), and the standardized root mean square residual (SRMR). Researchers have suggested various fit index cut-off criteria for a 'good fitting' model (Byrne, 1998; Hu and Bentler, 1999; Sugawara and MacCallum, 1993), but there is no single optimal cut-off for all types of models (Chen et al., 2008). However, these conventional cut-off criteria as originally proposed by Hu and Bentler (1999) are widely used: RMSEA < 0.06, CFI > 0.95, TLI > 0.95, and SRMR < 0.08.

One consequence of the structural model illustrated in Fig. 2 is the possibility of estimating an indirect effect between the latent network variable and the behavioral variable through the hypothesized ROI of interest. This is because the common association among the ROIs of the network (including the hypothesized ROI) are modeled as arising through the common causal relationship from the network to each ROI (i.e. the directed arrows from the network to the ROIs), and the hypothesized ROI is modeled as causally influencing the behavioral variable. Thus, a possible indirect effect may be estimated, which can be viewed as travelling from the network to the hypothesized ROI, and from the hypothesized ROI to the behavioral variable. This would represent a sort of 'top-down' influence of the network on ROI-behavior association, which may be of interest in future applications of this model. However, given the stated goal of the model to estimate unique network- and ROI-level brain-behavior associations, the two direct effect parameters, from the ROI to the behavioral variable and from the latent network variable to the behavioral variable, are the only parameters of interest in this application.

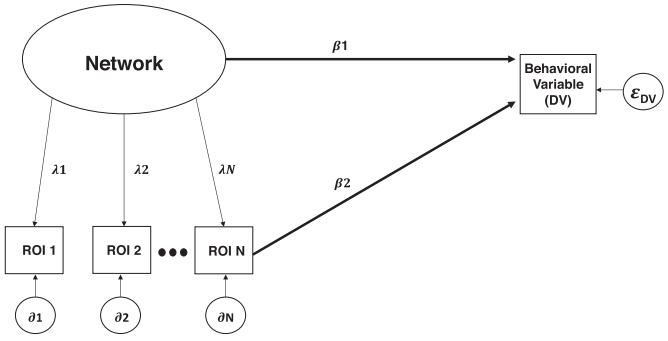

Fig. 2. Path Diagram of ROI-Network Structural Regression Model. Path diagram illustrating the parameters estimated in the proposed structural regression model. The measurement component corresponds to the left side of the figure, with paths proceeding from the latent variable representing latent network activity (represented by an oval) to each constituent ROI (represented by square boxes). The structural component corresponds to the right side of the figure, with paths proceeding from both the latent network variable and hypothesized ROI (e.g. ROI N) to the behavioral variable of interest (e.g. task accuracy). The structural paths represent 'causal' paths from the latent network variable and hypothesized ROI to the behavioral variable, and are distinct from the paths proceeding from the latent network variable to the ROIs in the measurement model (distinguished from the measurement model by thicker lines). Formal interpretations of each parameter in the model are described in Eq. (1) and Eq. (2).

This SEM framework was applied separately to the working memory, relational and auditory arithmetic task datasets. In all three tasks, the measurement component consisted of a CFA that modeled activation in the constituent ROIs (including the hypothesized ROI) of the FPN or CO/S network as a linear function of latent FPN or CO/S activation estimates. For the working memory task and relational task, all ROIs of the FPN in the Power (N = 25) and Gordon (N = 24) parcellation were included in the analysis. For the arithmetic task, all ROIs of the S/CO network in the Power (N = 18) and Gordon (N = 40) parcellation were included in the analysis. The structural component consisted of a path analysis model specifying causal relationships between the FPN or CO/S latent network variable and task accuracy, and between the hypothesized ROI and task accuracy. Results for the path coefficients were evaluated for significance using a conventional *alpha* level ($p < 0.05$).

Results

Analysis of ROI-Behavior association

Accuracy scores reached acceptable average levels (i.e. above chance − 50%) and demonstrated sufficient across-participant variability for the working memory task (M = 81.94%, *SD* = 11.7%), relational task (*M* = 64.02%, *SD* = 18.07%), and auditory arithmetic task (*M* = 82.15%, *SD* = 9.67%). As sufficient across-participant variability in accuracy scores is required in order to predict variability in these scores, we chose tasks that had less than 100% accuracy for the majority of participants. The data from all three tasks were then screened to check for outliers and multivariate normality. Z-scores were used to determine whether univariate outliers impacted the distribution of accuracy scores in the working memory, relational and arithmetic tasks. For the relational and arithmetic task, all z-scores were within 3 standard deviations from the mean. For the working memory task, three of the participants had accuracy scores with more than three standard deviations below the mean. However, the skewness and kurtosis of working memory accuracy scores was within the limits of a normal distribution (Skewness = −0.95, SE = 0.172; Kurtosis = 0.821, SE = 0.341), and examination of Cook's difference scores (Cook and Weisberg, 1982) revealed that the three scores did not constitute multivariate outliers.

To provide an initial assessment of the ROI-behavior association without implementation of the SEM framework, a simple *Pearson* correlation was computed between the hypothesized ROIs and task accuracy for all three tasks. Consistent with previous studies, activation estimates of the hypothesized ROIs from both parcellations were significantly positively correlated with task accuracy. For the working memory task, there was a significant positive association between activation estimates in the right DLPFC and 2-back accuracy (Power: $r(198) = 0.33$, $p < 0.0001$; Gordon: $r(198) = 0.36$, $p < 0.0001$). For the relational task, there was a significant positive association between the activation estimates in the left RLPFC and relational accuracy (Power: $r(195) = 0.15$, $p = 0.03$; Gordon: $r(195) = 0.22$, $p = 0.0018$). For the auditory arithmetic task, there was a significant positive association between activation estimates in the right TPJ and arithmetic accuracy (Power: $r(194) = 0.18$, $p = 0.01$; Gordon: $r(194) = 0.27$, $p = 0.0001$).

ROI-network dependencies

The ROI-behavior associations indicate a relationship between activity in these regions of the brain and task performance. However, a *Pearson* correlation (zero-order correlation) between a single ROI and task performance fails to account for the dependencies among ROIs of the same network. To illustrate the dependencies among ROIs across the whole-brain and within networks, we computed a whole-brain correlation matrix representing the across-subject *Pearson* correlations between all 264 ROIs of the Power parcellation and 333 ROIs of the Gordon parcellation. As illustrated in Fig. 3, there are strong dependencies across many ROIs of the cortex, particularly in ROIs of the same network.

SEM results

To account for the common associations between the hypothesized ROIs (right DLPFC, left RLPFC, and right TPJ) and other ROIs of the FPN and CO/S network, we implemented a latent variable SEM framework. As described above, the SEM framework involved a structural regression model with two components: a measurement component modeling network activity as a latent variable with the constituent ROIs of the network as indicators, and a structural component modeling the unique association of both the latent network and hypothesized ROI activation estimates with task accuracy. First, the measurement model was estimated to determine the relationship between each hypothesized ROI and its corresponding overall latent network (FPN or CO/S). After the measurement model was checked for possible low loading ROI-network paths ($\lambda \leq 0.5$), the structural model, including the paths from the network and hypothesized ROI to task accuracy, were added and the full model was estimated.

The SEM structural regression approach was first applied to the working memory task. This tested whether the original association between the right DLPFC and task accuracy holds after considering the right DLPFC's common association with other ROIs of the FPN. In addition, the model estimated the association between overall FPN activation estimates and task accuracy. First, a CFA model was fit to the data with all ROIs (n = 25 for the Power parcellation; n = 23 for the Gordon parcellation) of the FPN, including the ROI in the right DLPFC, as indicators of a latent FPN variable, representing overall FPN activity. Examination of the network-ROI factor loadings (Table 1), representing the correlation between activation estimates of the FPN and constituent ROIs, revealed that all ROIs for both parcellations had strong loadings on the FPN latent variable ($\lambda > 0.5$, $p < 0.0001$), excluding two ROIs from the Gordon parcellation, which were removed from the model due to their weak ROI-Network loadings ($\lambda \leq 0.5$). Thus, activation estimates within each of the ROIs had a strong association with overall activation estimates in the FPN. After adding residual covariance parameters between several of the ROIs (ratio of number of covariance parameters added to possible number of covariance parameters: Power = 49/300; Gordon = 58/231), the hypothesized model achieved acceptable levels of overall fit for both the Power (*RMSEA* = 0.059; *SRMR* = 0.041; *CFI* = 0.96; *TLI* = 0.947) and Gordon parcellations (*RMSEA* = 0.062; *SRMR* = 0.039; *CFI* = 0.971; *TLI* = 0.957). The final model with both measurement and structural components (paths added between the hypothesized ROI/FPN and task accuracy) was then fit to the data (Fig. 4). For both parcellations, the results of the final model (standardized results) revealed that the FPN was strongly positively associated with 2-back accuracy (Power: $B = 0.522$, $SE = 0.099$, $p < 0.0001$; Gordon: $B = 0.532$, $SE = 0.123$, $p < 0.0001$). In contrast to the analysis between the right DLPFC and 2-back accuracy, activation estimates in the right DLPFC in the structural model were no longer significantly associated with 2-back accuracy (Power: $B = -0.109$, $SE = 0.129$, $p = 0.4$; Gordon: $B = -0.1$, $SE = 0.129$, $p = 0.44$).

The SEM structural regression approach was then applied to the relational task. Examination of the network-ROI factor loadings (Table 1) revealed that all ROIs for both parcellations had strong loadings on the FPN latent variable ($\lambda's > 0.5$, $p's < 0.0001$). After adding residual covariance parameters between several of the network ROIs (ratio of number of covariance parameters added to possible number of covariance parameters: Power = 46/300; Gordon = 36/276), the hypothesized model achieved acceptable levels of overall fit for both the Power (*RMSEA* = 0.061; *SRMR* = 0.036; *CFI* = 0.966; *TLI* = 0.955) and Gordon parcellations (*RMSEA* = 0.061; *SRMR* = 0.031; *CFI* = 0.971; *TLI* = 0.962). The final model with both measurement and structural components (paths added between ROI-FPN and task accuracy) was then fit to the data (Fig. 4). Similar to the working memory task, the results of the final model revealed a different interpretation of the relationship between activation estimates in the left RLPFC and relational accuracy than the original analysis with a single ROI. For both parcellations, the results of the final model revealed that the FPN was strongly positively associated with relational accuracy (Power: $B = 0.697$, $SE = 0.077$, $p < 0.0001$; Gordon: $B = 0.53$, $SE = 0.095$, $p < 0.0001$). In contrast to the original *positive* correlation, activation estimates in the left RLPFC had a weak *negative* association with relational accuracy in the Power parcellation ($B = -0.377$, $SE = 0.09$, $p < 0.0001$), and a non-significant negative association in the Gordon parcellation ($B = -0.19$, $SE = 0.047$, $p = 0.085$).

The SEM structural regression approach was then applied to the auditory arithmetic task. Examination of the network-ROI factor loadings (Table 1) revealed that many ROIs for the Power (n = 14) and Gordon (n = 34) parcellations had strong loadings on the Salience, and Cingulo-Opercular network latent variable ($\lambda's > 0.5$, $p's < 0.0001$), respectively. Four ROIs of the Power parcellation, and six ROIs of the Gordon parcellation did not exhibit strong network-ROI factor loadings ($\lambda < 0.5$) and were excluded from further analyses. Of note, the right TPJ in the Power parcellation was marginally below the network-ROI factor loading threshold ($\lambda = 0.494$), but was maintained in the model as this was the hypothesized region of interest. After adding residual covariance parameters between several of the network ROIs (ratio of number of covariance parameters added to possible number of covariance parameters: Power = 8/91; Gordon = 80/595), the hypothesized model achieved acceptable levels of overall fit for both the Power (*RMSEA* = 0.053; *SRMR* = 0.042; *CFI* = 0.969; *TLI* = 0.96) and Gordon parcellations (*RMSEA* = 0.055; *SRMR* = 0.057; *CFI* = 0.943; *TLI* = 0.928). The final model with both measurement and structural components (paths added between ROI-CO/S and task accuracy) was then fit to the data (Fig. 4). For both parcellations, the results of the final model revealed that the overall network activation estimates were not significantly associated with arithmetic accuracy (Power: $B = 0.071$, $SE = 0.079$, $p = 0.368$; Gordon: $B = -0.022$, $SE = 0.092$, $p = 0.807$). In agreement with the earlier results, a positive association with activation estimates in the right TPJ and arithmetic accuracy remained in the Gordon parcellation ($B = 0.287$, $SE = 0.094$, $p = 0.002$), though the positive association with activation estimates in the right TPJ and arithmetic accuracy was non-significant in the Power parcellation ($B = 0.145$, $SE = 0.079$, $p = 0.064$). This is in direct contrast to the findings for the auditory arithmetic and working memory tasks, which revealed an overall network activation estimate which had a distinct impact on the original *Pearson* correlation.

Discussion

In this study, we demonstrate the utility of an SEM framework for incorporating region- and network-level brain-behavior associations in a single model. This framework allowed us to estimate the unique contribution of hypothesized ROIs, and compare those associations with the contribution of the overall network. Applied to three separate task-fMRI datasets, we found that the approach yielded fundamentally different insights into brain-behavior correlates compared with a traditional ROI brain-behavior correlation. For the working memory and relational task, we found that the unique associations between hypothesized ROIs and task accuracy were *negative* once the corresponding network influence was controlled, and that the network activation significantly predicted task accuracy. In the auditory arithmetic task, the association between the hypothesized ROI and task accuracy was maintained even when accounting for its common association with its network, and network activation estimates were not robustly predictive of task accuracy.

These findings illustrate the importance of accounting for dependencies among levels of analyses, as well as the unique insights offered by each level considered separately. Previous fMRI studies of working memory processes (Barbey et al., 2013; Barch et al., 1997; Curtis & D'Esposito, 2003; Owen et al., 2005; Rypma & D'Esposito, 1999) have generally implicated either a single ROI (e.g. DLPFC) or other sets of ROIs associated with the FPN. The SEM framework applied to the working memory dataset incorporated both aspects in a single model, and

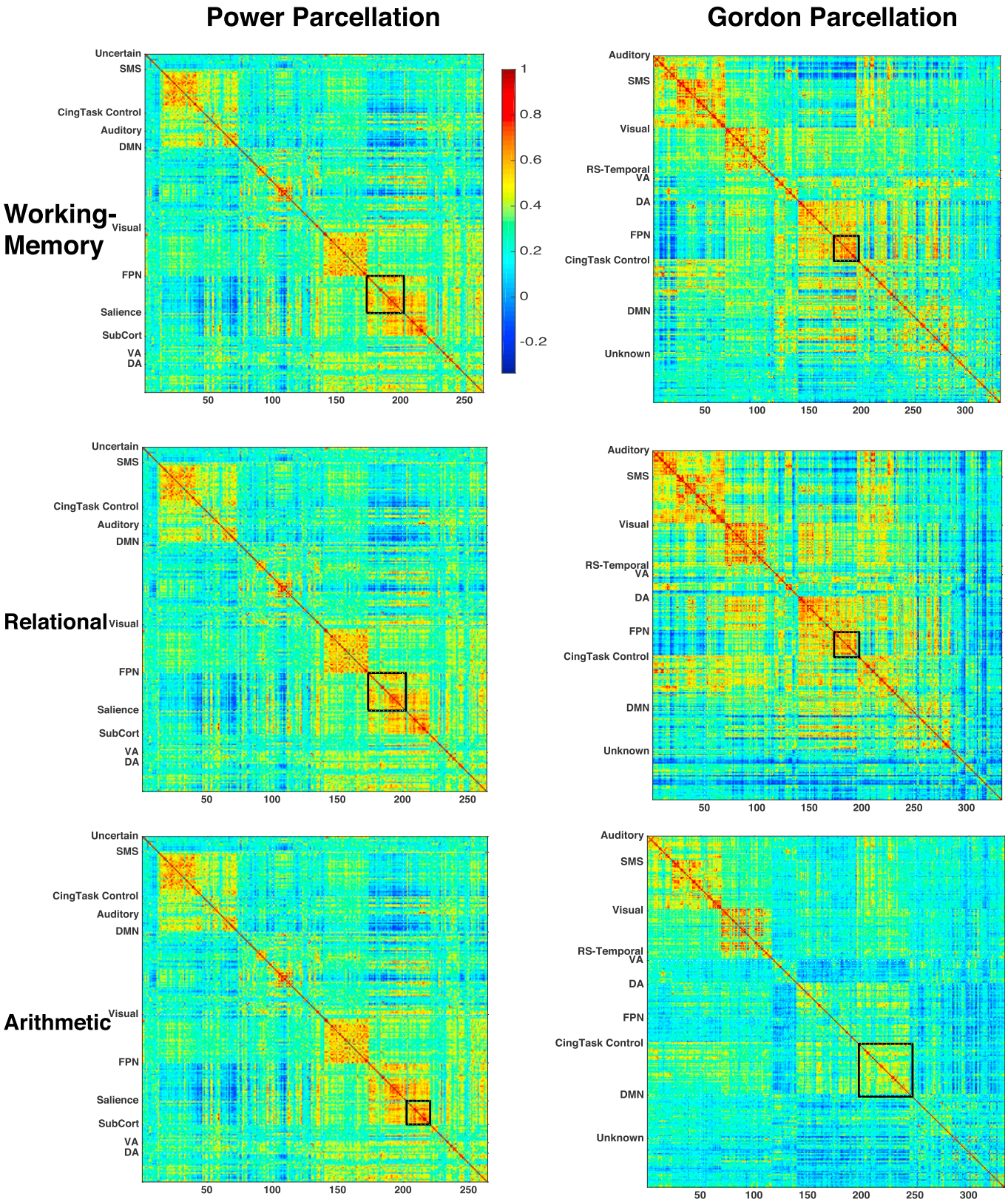

Fig. 3. Across-Subject Correlation Matrices of All ROIs in Three Tasks. (Network labels: SMS = Somatosensory Network, CingTask Control = Cingulo-opercular Network, RS-Temporal = Retrosplenial-Temporal Network DMN = Default Mode Network, FPN = Fronto-Parietal Network, SubCort = Subcortical Network, VA = Ventral Attention Network, and DA = Dorsal Attention Network). Correlation matrices of the correlations of activation values across subjects between all 264 ROIs of the Power parcellation and 333 ROIs of the Gordon parcellation. Correlation estimates are displayed with a heat map: warmer colors (red) represent stronger positive correlations and cooler colors (blue) represent weak positive to negative correlations. Network labels are presented along the vertical axis of the matrix, and node numbering is presented along the horizontal axis. Networks of interest (FPN and CO/S) are outlined in black boxes. Examination of the correlation matrix reveals that there are prevalent dependencies among the ROIs, particularly for ROIs within the same network.

Table 1
Network-ROI Factor Loadings for All Three Tasks Across Power and Gordon Parcellations. (λ = factor loadings; WM = Working Memory Task). Table of factor loadings for each ROI across both parcellations, representing the correlation of overall activation estimates of the FPN (for working memory and relational task) and CO/S network (for arithmetic task) with ROI activation estimates, as well as associated standard errors (all p's < 0.0001). Of note, these are the factor loadings *after* the covariance parameters were added the measurement model. The hypothesized ROIs from each parcellation for each task are presented in bold letter.

Power Parcellation									Gordon Parcellation								
WM			Relational			Arithmetic			WM			Relational			Arithmetic		
ROI	λ	SE	ROI	λ	SE	ROI	λ	SE	ROI	λ	SE	ROI	λ	SE	ROI	λ	SE
1	0.776	0.029	1	0.739	0.032	1	0.512	0.062	1	0.565	0.066	1	0.791	0.031	1	0.709	0.038
2	0.768	0.03	2	0.835	0.025	**2**	0.494	0.068	2	0.721	0.036	2	0.718	0.043	2	0.695	0.045
3	0.689	0.044	3	0.796	0.027	3	0.571	0.056	3	0.839	0.022	3	0.885	0.016	3	0.742	0.03
4	0.721	0.039	4	0.839	0.021	4	0.542	0.064	4	0.765	0.041	**4**	0.792	0.025	4	0.664	0.044
5	0.713	0.041	5	0.825	0.025	5	0.661	0.042	5	0.732	0.03	5	0.872	0.017	5	0.595	0.05
6	0.616	0.05	6	0.783	0.029	6	0.715	0.044	6	0.609	0.049	6	0.844	0.021	6	0.506	0.052
7	0.538	0.055	7	0.553	0.055	7	0.638	0.055	7	0.818	0.027	7	0.807	0.023	7	0.59	0.048
8	0.645	0.048	8	0.566	0.06	8	0.728	0.039	8	1.064	0.071	8	0.656	0.044	8	0.736	0.038
9	0.786	0.029	9	0.857	0.022	9	0.751	0.038	9	0.607	0.068	9	0.797	0.033	9	0.698	0.043
10	0.749	0.033	10	0.828	0.024	10	0.834	0.025	10	0.652	0.041	10	0.867	0.021	10	0.652	0.051
11	0.607	0.05	11	0.795	0.026	11	0.809	0.033	11	0.874	0.022	11	0.822	0.028	11	0.65	0.043
12	0.712	0.037	12	0.754	0.037	12	0.701	0.042	12	0.752	0.033	12	0.771	0.03	12	0.576	0.055
13	0.849	0.023	13	0.85	0.023	13	0.544	0.06	13	0.831	0.024	13	0.895	0.016	13	0.548	0.061
14	0.773	0.032	14	0.83	0.025	14	0.587	0.057	14	0.951	0.054	14	0.729	0.032	14	0.571	0.054
15	0.85	0.023	15	0.893	0.026				15	0.882	0.017	15	0.887	0.022	15	0.688	0.046
16	0.85	0.024	16	0.881	0.017				16	0.749	0.035	16	0.837	0.024	16	0.707	0.042
17	0.803	0.026	17	0.855	0.02				17	0.726	0.03	17	0.877	0.02	17	0.637	0.05
18	0.836	0.024	18	0.902	0.014				18	0.807	0.028	18	0.882	0.018	18	0.745	0.035
19	0.832	0.024	19	0.841	0.02				19	0.804	0.026	19	0.726	0.04	19	0.619	0.053
20	0.772	0.032	20	0.802	0.032				20	0.707	0.054	20	0.735	0.037	20	0.757	0.037
21	0.716	0.032	**21**	0.766	0.026				**21**	0.888	0.017	21	0.696	0.043	21	0.509	0.066
22	0.761	0.028	22	0.8	0.03				22	0.64	0.056	22	0.853	0.021	22	0.657	0.051
23	0.668	0.046	23	0.648	0.039							23	0.918	0.013	23	0.636	0.051
24	0.8	0.031	24	0.873	0.017							24	0.838	0.023	**24**	0.655	0.051
25	0.861	0.021	25	0.892	0.015										25	0.668	0.048
															26	0.592	0.061
															27	0.67	0.04
															28	0.696	0.046
															29	0.691	0.043
															30	0.623	0.056
															31	0.683	0.046
															32	0.709	0.038
															33	0.546	0.055
															34	0.713	0.041

revealed that right DLPFC activation is subsumed by overall activity in the FPN. Previous fMRI studies of relational processing (Badgaiyan et al., 2002; Bunge et al., 2009; Christoff et al., 2001) have implicated the left RLPFC as uniquely related to relational task processing. But as demonstrated by application of the SEM framework, the original positive association between left RLPFC activation estimates and task performance was *reversed* when accounting for its association with the FPN in the Power parcellation (this reversal was non-significant in the Gordon parcellation, $p = 0.085$). Overall, these results suggest that the unit of behavioral significance in the brain for these specific cognitive control tasks, and possibly for others, is the FPN, rather than a single ROI within this network. The auditory arithmetic task provides an instance of a case when the hypothesized ROI, the right TPJ, is uniquely related to task performance, as opposed to its entire associated network. In this case, the unique activity of the right TPJ in the Gordon parcellation (this association was non-significant in the Power parcellation, $p = 0.064$) is related to task accuracy while its associated network is not. Thus, under some circumstances the ROI-specific activation maintains a unique relationships with task performance, even when controlling for the relationship with its associated network. However, these results are dependent on carefully choosing the ROI (as in all ROI analyses; Poldrack, 2007), as the relationship between the hypothesized ROI in the Power parcellation and task-performance was non-significant ($p = 0.064$). This may be due to the fact that the right TPJ in the Power parcellation did not have a strong association with its associated network ($\lambda = 0.494$).

Several studies have demonstrated that task co-activation patterns form networks of co-varying brain regions, similar to those observed in resting-state fMRI (Crossley et al., 2013; Laird et al., 2013; Smith et al., 2009). A similar pattern of network structure was observed among the ROI task co-activation patterns for the three tasks used in the current study (Fig. 3). The results of the SEM framework applied to the three tasks demonstrate the importance of assessing both networks of ROIs and individual ROIs and their relationships to behavioral variables of interest (Leergaard et al., 2012; Poldrack and Farah, 2015). The SEM framework explored here provides a simple approach for parsing the unique contributions of ROI- and network-level activity. This approach operates by modeling the common associations among regions of the same network, and simultaneously estimating the unique contributions of both the overall network and the hypothesized ROI to a behavioral variable of interest.

While the SEM framework in this study was applied to task fMRI data, individual differences in resting-state functional connectivity estimates between hypothesized ROIs are an increasingly popular source of brain data for studies of brain-behavior relationships (Aghajani et al., 2014; Disbrow et al., 2014; Hampson et al., 2006; Krmpotich et al., 2013; Vossel et al., 2016; Wang et al., 2007). Analogous to the concerns of ROI-network dependencies in task-activation data, functional connectivity relationships between hypothesized ROIs may be dependent on relationships among larger networks of regions. The SEM framework in this study operated on *across-subject* correlations in ROI task-activation estimates at the *between-subject* level, while resting-state functional connectivity estimates are commonly estimated at the *within-subject* level. Applications of the SEM framework on within-subject resting-state functional connectivity estimates would require an extension of the SEM

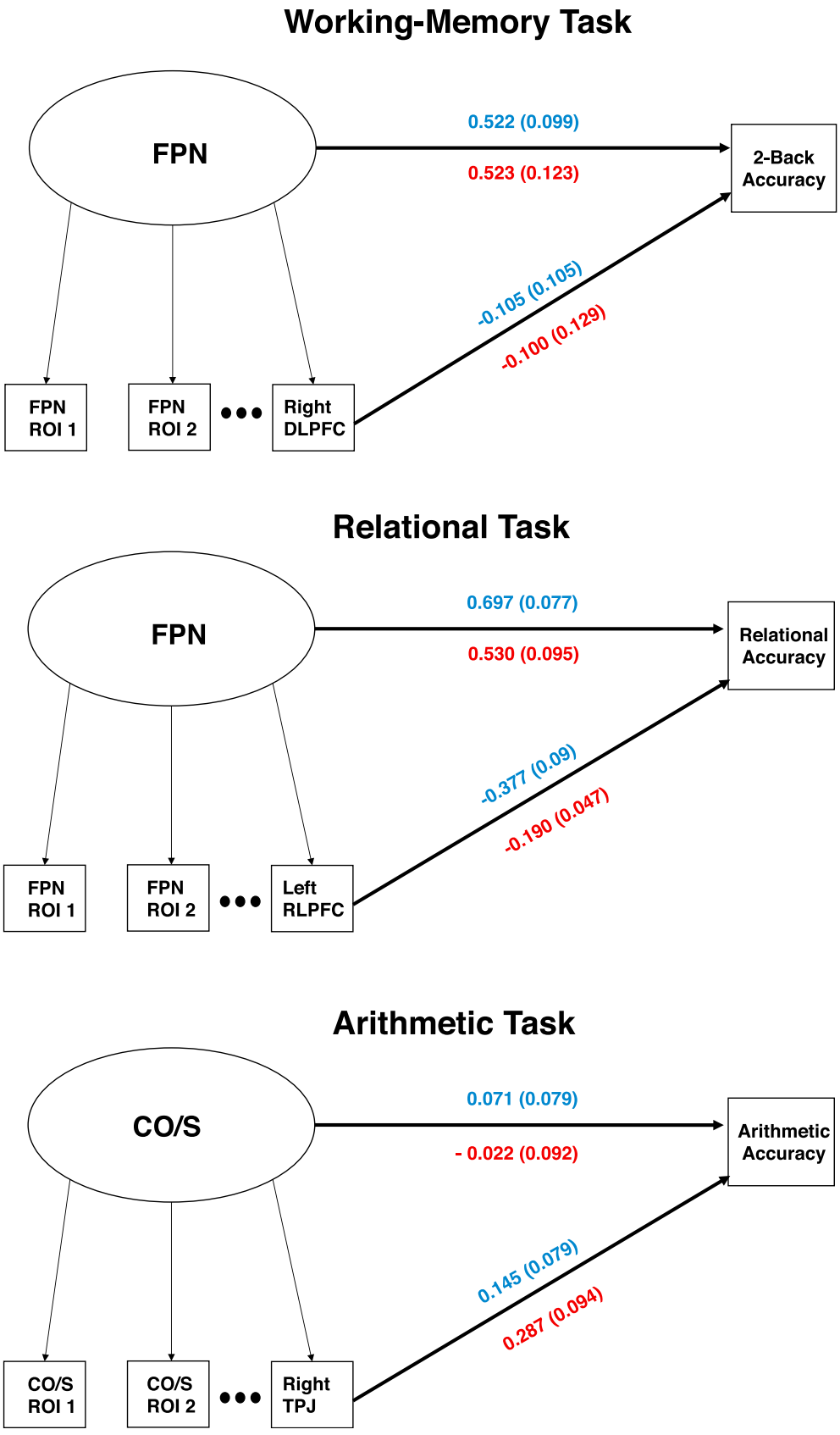

Fig. 4. Parameter Estimates of Structural Regression Model. (FPN = Fronto-Parietal Network, CO/S = Cingulo-opercular/Salience Network). Path diagrams with standardized parameter estimates (standard errors presented in parentheses) for two paths: 1) the path between the latent network variable and task accuracy, representing the unique association between overall activation estimates in the FPN or CO/S network and task accuracy, and 2) the path between the hypothesized ROI (right DLPFC/left RLPFC/right TPJ) and task accuracy, representing the association between residual activation estimates in the ROI (activity due to association with the network removed) and task accuracy. Power parcellation estimates are presented in blue, and Gordon parcellation estimates are presented in red.

framework to *multi-level* data: estimates at the within-subject level would need to be extended to the between-subject level to predict individual differences, accounting for both within- and between-subject variability. Fortunately, software for multi-level SEM approaches are widely available (Preacher et al., 2010; Rabe-Hesketh et al., 2004; Toit & Toit, 2008). Future studies are needed to determine the applicability of this SEM framework to resting-state functional connectivity-based brain-behavior relationships.

Limitations

The results of the SEM approach here highlight the need for accounting for the hierarchical functional organization of the human brain when conducting brain-behavior associations in task fMRI. However, this approach is still limited to *hypothesis-driven* research, requiring researchers to specify *a priori* the brain regions of interest that are associated with task performance. This requires informed choices by the researcher based on previous findings and well-reasoned hypotheses, as opposed to a more data-driven approach. In addition, this requires an *a priori* specification of ROI-network membership, where the hypothesized ROI along with all other ROIs in its associated network are included in the model. This can perhaps be best derived from previous fMRI parcellation studies (Bassett et al., 2008; Meunier et al., 2010; Yeo et al., 2011), including the ones used in this study (Gordon et al., 2016; Power et al., 2011). This is a non-trivial choice, as the creation of the network latent variable is dependent on the chosen ROIs that constitute the network. This is the primary reason that two network parcellations were used in the current study (Gordon et al., 2016; Power et al., 2011). As shown in the arithmetic task, different parcellation schemes can sometimes yield different results in terms of the significance ($p < 0.05$) of the path estimates. Rather than using an *a priori* parcellation, data-driven estimation techniques on one's own data (e.g. ICA) may provide more robust estimations of network-ROI membership for future applications of this SEM approach. Related to this issue, is the well-noted fact that multiple SEM models can fit the data equally well (Hu and Bentler, 1998; Iacobucci, 2010; Steiger, 2007). This highlights the importance of *hypothesis-driven* applications of the SEM framework to brain-behavior association studies. Adjudicating between different models requires that researchers also discern the neurobiological meaning of these models, such that relationships among model variables are theoretically grounded.

As noted above, several covariance parameters were added to the ROI-Network measurement model to achieve adequate levels of model fit. Though the common network membership accounts for the majority of variance in the ROIs, the addition of covariance parameters to the model indicate there are extra dependences in the model not accounted for by network membership. These extra dependencies among ROIs could possibly be the result of spatial dependencies between nearby ROIs, homologous ROIs from the right and left hemisphere, or 'sub-networks' within the overall network. Though these are captured by the added covariance parameters, future applications of this approach may choose to more systematically account for these dependencies with extra path estimates, or possibly a bi-factor CFA model that models a general factor, and sub-factors within this factor (Reise, 2012; Reise et al., 2007).

Conclusions

Here we demonstrate the importance of accounting for both ROI- and network-levels of analysis in studies of brain-behavior relationships. The contributions of multiple levels of analysis in the brain should be taken into consideration when predicting individual differences in behavior from fMRI data. Additional research is needed to understand how these different levels of analysis in the brain interact, and how they differentially contribute to cognitive processes and behavioral outcomes. An understanding of what level of analysis contributes most to a behavioral outcome of interest is particularly important for those researchers concerned with subject-level fMRI biomarkers for clinical and disease outcomes. We believe that the framework described in this study will allow researchers additional flexibility in testing of brain-behavior relationships, as well as a principled way to combine ROI- and network-levels of analysis.

Acknowledgments

This work was supported by the National Institute of Mental Health (R01MH107549) to LQU and a University of Miami Convergence Research Grant to DM and LQU.

Appendix A. Supplementary data

Supplementary data related to this article can be found at https://doi.org/10.1016/j.neuroimage.2017.10.007.

References

Aghajani, M., Veer, I.M., van Tol, M.-J., Aleman, A., van Buchem, M.A., Veltman, D.J., van der Wee, N.J., 2014. Neuroticism and extraversion are associated with amygdala resting-state functional connectivity. Cogn. Affect. Behav. Neurosci. 14 (2), 836–848. https://doi.org/10.3758/s13415-013-0224-0.

Ansari, D., 2008. Effects of development and enculturation on number representation in the brain. Nat. Rev. Neurosci. 9 (4), 278–291. https://doi.org/10.1038/nrn2334.

Badgaiyan, R.D., Schacter, D.L., Alpert, N.M., 2002. Retrieval of relational information: a role for the left inferior prefrontal cortex. NeuroImage 17 (1), 393–400.

Barbey, A.K., Koenigs, M., Grafman, J., 2013. Dorsolateral prefrontal contributions to human working memory. Cortex J. Devoted Study Nerv. Syst. Behav. 49 (5), 1195–1205. https://doi.org/10.1016/j.cortex.2012.05.022.

Barch, D.M., Braver, T.S., Nystrom, L.E., Forman, S.D., Noll, D.C., Cohen, J.D., 1997. Dissociating working memory from task difficulty in human prefrontal cortex. Neuropsychologia 35 (10), 1373–1380. https://doi.org/10.1016/S0028-3932(97)00072-9.

Barch, D.M., Burgess, G.C., Harms, M.P., Petersen, S.E., Schlaggar, B.L., Corbetta, M., WU-Minn HCP Consortium, 2013. Function in the human connectome: task-fMRI and individual differences in behavior. NeuroImage 80, 169–189. https://doi.org/10.1016/j.neuroimage.2013.05.033.

Bassett, D.S., Bullmore, E., Verchinski, B.A., Mattay, V.S., Weinberger, D.R., Meyer-Lindenberg, A., 2008. Hierarchical organization of human cortical networks in health and Schizophrenia. J. Neurosci. 28 (37), 9239–9248. https://doi.org/10.1523/JNEUROSCI.1929-08.2008.

Beaty, R.E., Kaufman, S.B., Benedek, M., Jung, R.E., Kenett, Y.N., Jauk, E., Silvia, P.J., 2016. Personality and complex brain networks: the role of openness to experience in default network efficiency. Hum. Brain Mapp. 37 (2), 773–779. https://doi.org/10.1002/hbm.23065.

Bentler, P.M., 2007. On tests and indices for evaluating structural models. Pers. Individ. Differ. 42 (5), 825–829. https://doi.org/10.1016/j.paid.2006.09.024.

Bullmore, E., Sporns, O., 2009. Complex brain networks: graph theoretical analysis of structural and functional systems. Nat. Rev. Neurosci. 10 (3), 186–198. https://doi.org/10.1038/nrn2575.

Bunge, S.A., Helskog, E.H., Wendelken, C., 2009. Left, but not right, rostrolateral prefrontal cortex meets a stringent test of the relational integration hypothesis. NeuroImage 46 (1), 338–342. https://doi.org/10.1016/j.neuroimage.2009.01.064.

Butterworth, B., Walsh, V., 2011. Neural basis of mathematical cognition. Curr. Biol. 21 (16), R618–R621. https://doi.org/10.1016/j.cub.2011.07.005.

Byrne, B.M., 1998. Structural Equation Modeling with Lisrel, Prelis, and Simplis: Basic Concepts, Applications, and Programming, 1 edition. Psychology Press, Mahwah, N.J.

Calhoun, V.D., Kiehl, K.A., Pearlson, G.D., 2008. Modulation of temporally coherent brain networks estimated using ICA at rest and during cognitive tasks. Hum. Brain Mapp. 29 (7), 828–838. https://doi.org/10.1002/hbm.20581.

Chen, F., Curran, P.J., Bollen, K.A., Kirby, J., Paxton, P., 2008. An empirical evaluation of the use of fixed cutoff points in RMSEA test statistic in structural equation models. Sociol. Methods & Res. 36 (4), 462–494. https://doi.org/10.1177/0049124108314720.

Christoff, K., Prabhakaran, V., Dorfman, J., Zhao, Z., Kroger, J.K., Holyoak, K.J., Gabrieli, J.D.E., 2001. Rostrolateral prefrontal cortex involvement in relational integration during reasoning. NeuroImage 14 (5), 1136–1149. https://doi.org/10.1006/nimg.2001.0922.

Clarke, K.A., 2005. The phantom menace: omitted variable bias in econometric research. Confl. Manag. Peace Sci. 22 (4), 341–352. https://doi.org/10.1080/07388940500339183.

Cole, D.M., Smith, S.M., Beckmann, C.F., 2010. Advances and pitfalls in the analysis and interpretation of resting-state FMRI data. Front. Syst. Neurosci. 4 https://doi.org/10.3389/fnsys.2010.00008.

Cole, M.W., Reynolds, J.R., Power, J.D., Repovs, G., Anticevic, A., Braver, T.S., 2013. Multi-task connectivity reveals flexible hubs for adaptive task control. Nat. Neurosci. 16 (9), 1348–1355. https://doi.org/10.1038/nn.3470.

Comrey, A.L., Lee, H.B., 1992. A First Course in Factor Analysis, second ed. Psychology Press, Hillsdale, N.J.

Cook, R.D., Weisberg, S., 1982. Residuals and Influence in Regression. Chapman & Hall.
Crossley, N.A., Mechelli, A., Vértes, P.E., Winton-Brown, T.T., Patel, A.X., Ginestet, C.E., Bullmore, E.T., 2013. Cognitive relevance of the community structure of the human brain functional coactivation network. Proc. Natl. Acad. Sci. 110 (28), 11583–11588. https://doi.org/10.1073/pnas.1220826110.
Curtis, C.E., D'Esposito, M., 2003. Persistent activity in the prefrontal cortex during working memory. Trends Cogn. Sci. 7 (9), 415–423. https://doi.org/10.1016/S1364-6613(03)00197-9.
Damoiseaux, J.S., Rombouts, S.a.R.B., Barkhof, F., Scheltens, P., Stam, C.J., Smith, S.M., Beckmann, C.F., 2006. Consistent resting-state networks across healthy subjects. Proc. Natl. Acad. Sci. 103 (37), 13848–13853. https://doi.org/10.1073/pnas.0601417103.
de Marco, G., Vrignaud, P., Destrieux, C., de Marco, D., Testelin, S., Devauchelle, B., Berquin, P., 2009. Principle of structural equation modeling for exploring functional interactivity within a putative network of interconnected brain areas. Magn. Reson. Imaging 27 (1), 1–12. https://doi.org/10.1016/j.mri.2008.05.003.
Disbrow, E.A., Carmichael, O., He, J., Lanni, K.E., Dressler, E.M., Zhang, L., Sigvardt, K.A., 2014. Resting state functional connectivity is associated with cognitive dysfunction in non-demented people with Parkinson's disease. J. Parkinson's Dis. 4 (3), 453–465. https://doi.org/10.3233/JPD-130341.
Doucet, G., Naveau, M., Petit, L., Delcroix, N., Zago, L., Crivello, F., Joliot, M., 2011. Brain activity at rest: a multiscale hierarchical functional organization. J. Neurophysiol. 105 (6), 2753–2763. https://doi.org/10.1152/jn.00895.2010.
Fan, X., Thompson, B., Wang, L., 1999. Effects of sample size, estimation methods, and model specification on structural equation modeling fit indexes. Struct. Equ. Model. A Multidiscip. J. 6 (1), 56–83. https://doi.org/10.1080/10705519909540119.
Ferrarini, L., Veer, I.M., Baerends, E., van Tol, M.-J., Renken, R.J., van der Wee, N.J.A., Milles, J., 2009. Hierarchical functional modularity in the resting-state human brain. Hum. Brain Mapp. 30 (7), 2220–2231. https://doi.org/10.1002/hbm.20663.
Fornito, A., Harrison, B.J., Zalesky, A., Simons, J.S., 2012. Competitive and cooperative dynamics of large-scale brain functional networks supporting recollection. Proc. Natl. Acad. Sci. 109 (31), 12788–12793. https://doi.org/10.1073/pnas.1204185109.
Fox, M.D., Snyder, A.Z., Vincent, J.L., Corbetta, M., Essen, D.C.V., Raichle, M.E., 2005. The human brain is intrinsically organized into dynamic, anticorrelated functional networks. Proc. Natl. Acad. Sci. U. S. A. 102 (27), 9673–9678. https://doi.org/10.1073/pnas.0504136102.
Friston, K.J., Harrison, L., Penny, W., 2003. Dynamic causal modelling. NeuroImage 19 (4), 1273–1302. https://doi.org/10.1016/S1053-8119(03)00202-7.
Gates, K.M., Molenaar, P.C.M., Hillary, F.G., Slobounov, S., 2011. Extended unified SEM approach for modeling event-related fMRI data. NeuroImage 54 (2), 1151–1158. https://doi.org/10.1016/j.neuroimage.2010.08.051.
Glasser, M.F., Sotiropoulos, S.N., Wilson, J.A., Coalson, T.S., Fischl, B., Andersson, J.L., WU-Minn HCP Consortium, 2013. The minimal preprocessing pipelines for the Human Connectome Project. NeuroImage 80, 105–124. https://doi.org/10.1016/j.neuroimage.2013.04.127.
Gordon, E.M., Laumann, T.O., Adeyemo, B., Huckins, J.F., Kelley, W.M., Petersen, S.E., 2016. Generation and evaluation of a cortical area parcellation from resting-state correlations. Cereb. Cortex (New York, N.Y. 1991), 26 (1), 288–303. https://doi.org/10.1093/cercor/bhu239.
Grabner, R.H., Ansari, D., Reishofer, G., Stern, E., Ebner, F., Neuper, C., 2007. Individual differences in mathematical competence predict parietal brain activation during mental calculation. NeuroImage 38 (2), 346–356. https://doi.org/10.1016/j.neuroimage.2007.07.041.
Hair, J.F., Black, W.C., Babin, B.J., Anderson, R.E., 2013. Multivariate Data Analysis. Pearson Education Limited.
Hampson, M., Driesen, N.R., Skudlarski, P., Gore, J.C., Constable, R.T., 2006. Brain connectivity related to working memory performance. J. Neurosci. 26 (51), 13338–13343. https://doi.org/10.1523/JNEUROSCI.3408-06.2006.
Hu, L., Bentler, P.M., 1998. Fit indices in covariance structure modeling: sensitivity to underparameterized model misspecification. Psychol. Methods 3 (4), 424–453. https://doi.org/10.1037/1082-989X.3.4.424.
Hu, L., Bentler, P.M., 1999. Cutoff criteria for fit indexes in covariance structure analysis: conventional criteria versus new alternatives. Struct. Equ. Model. A Multidiscip. J. 6 (1), 1–55. https://doi.org/10.1080/10705519909540118.
Hubbard, E.M., Arman, A.C., Ramachandran, V.S., Boynton, G.M., 2005. Individual differences among grapheme-color synesthetes: brain-behavior correlations. Neuron 45 (6), 975–985. https://doi.org/10.1016/j.neuron.2005.02.008.
Iacobucci, D., 2010. Structural equations modeling: fit Indices, sample size, and advanced topics. J. Consum. Psychol. 20 (1), 90–98. https://doi.org/10.1016/j.jcps.2009.09.003.
James, G.A., Kelley, M.E., Craddock, R.C., Holtzheimer, P.E., Dunlop, B., Nemeroff, C., Hu, X.P., 2009. Exploratory Structural Equation Modeling of Resting-state fMRI: applicability of group models to individual subjects. NeuroImage 45 (3), 778–787. https://doi.org/10.1016/j.neuroimage.2008.12.049.
Karunanayaka, P., Eslinger, P.J., Wang, J.-L., Weitekamp, C.W., Molitoris, S., Gates, K.M., Yang, Q.X., 2014. Networks involved in olfaction and their dynamics using independent component analysis and unified structural equation modeling. Hum. Brain Mapp. 35 (5), 2055–2072. https://doi.org/10.1002/hbm.22312.
Kim, J., Zhu, W., Chang, L., Bentler, P.M., Ernst, T., 2007. Unified structural equation modeling approach for the analysis of multisubject, multivariate functional MRI data. Hum. Brain Mapp. 28 (2), 85–93. https://doi.org/10.1002/hbm.20259.
Kriegeskorte, N., Simmons, W.K., Bellgowan, P.S., Baker, C.I., 2009. Circular analysis in systems neuroscience – the dangers of double dipping. Nat. Neurosci. 12 (5), 535–540. https://doi.org/10.1038/nn.2303.
Krmpotich, T.D., Tregellas, J.R., Thompson, L.L., Banich, M.T., Klenk, A.M., Tanabe, J.L., 2013. Resting-state activity in the left executive control network is associated with behavioral approach and is increased in substance dependence. Drug Alcohol Depend. 129 (1–2), 1–7. https://doi.org/10.1016/j.drugalcdep.2013.01.021.
Laird, A.R., Eickhoff, S.B., Rottschy, C., Bzdok, D., Ray, K.L., Fox, P.T., 2013. Networks of task co-activations. NeuroImage 80, 505–514. https://doi.org/10.1016/j.neuroimage.2013.04.073.
Leech, R., Kamourieh, S., Beckmann, C.F., Sharp, D.J., 2011. Fractionating the default mode network: distinct contributions of the ventral and dorsal posterior cingulate cortex to cognitive control. J. Neurosci. Off. J. Soc. Neurosci. 31 (9), 3217–3224. https://doi.org/10.1523/JNEUROSCI.5626-10.2011.
Leergaard, T.B., Hilgetag, C.C., Sporns, O., 2012. Mapping the connectome: multi-level analysis of brain connectivity. Front. Neuroinformatics 6. https://doi.org/10.3389/fninf.2012.00014.
MacCallum, R.C., Widaman, K.F., Zhang, S., Hong, S., 1999. Sample size in factor analysis. Psychol. Methods 4 (1), 84–99. https://doi.org/10.1037/1082-989X.4.1.84.
Meunier, D., Lambiotte, R., Bullmore, E.T., 2010. Modular and hierarchically modular organization of brain networks. Front. Neurosci. 4 https://doi.org/10.3389/fnins.2010.00200.
Mišić, B., Sporns, O., 2016. From regions to connections and networks: new bridges between brain and behavior. Curr. Opin. Neurobiol. 40, 1–7. https://doi.org/10.1016/j.conb.2016.05.003.
Molenberghs, P., Trautwein, F.-M., Böckler, A., Singer, T., Kanske, P., 2016. Neural correlates of metacognitive ability and of feeling confident: a large-scale fMRI study. Soc. Cogn. Affect. Neurosci. nsw093. https://doi.org/10.1093/scan/nsw093.
Muthén, L.K., Muthén, B.O., 2011. Mplus User's Guide, sixth ed. Muthén & Muthén, Los Angeles, CA.
Nelson, S.M., Savalia, N.K., Fishell, A.K., Gilmore, A.W., Zou, F., Balota, D.A., McDermott, K.B., 2016. Default mode network activity predicts early memory decline in healthy young adults aged 18–31. Cereb. Cortex 26 (8), 3379–3389. https://doi.org/10.1093/cercor/bhv165.
Owen, A.M., McMillan, K.M., Laird, A.R., Bullmore, E., 2005. N-back working memory paradigm: a meta-analysis of normative functional neuroimaging studies. Hum. Brain Mapp. 25 (1), 46–59. https://doi.org/10.1002/hbm.20131.
Peterson, R.A., 2000. A meta-analysis of variance accounted for and factor loadings in exploratory factor analysis. Mark. Lett. 11 (3), 261–275. https://doi.org/10.1023/A:1008191211004.
Poldrack, R.A., 2007. Region of interest analysis for fMRI. Soc. Cogn. Affect. Neurosci. 2 (1), 67–70. https://doi.org/10.1093/scan/nsm006.
Poldrack, R.A., Farah, M.J., 2015. Progress and challenges in probing the human brain. Nature 526 (7573), 371–379. https://doi.org/10.1038/nature15692.
Power, J.D., Cohen, A.L., Nelson, S.M., Wig, G.S., Barnes, K.A., Church, J.A., Petersen, S.E., 2011. Functional network organization of the human brain. Neuron 72 (4), 665–678. https://doi.org/10.1016/j.neuron.2011.09.006.
Preacher, K.J., Zyphur, M.J., Zhang, Z., 2010. A general multilevel SEM framework for assessing multilevel mediation. Psychol. Methods 15 (3), 209–233. https://doi.org/10.1037/a0020141.
Price, G.R., Mazzocco, M.M.M., Ansari, D., 2013. Why mental arithmetic counts: brain activation during single digit arithmetic predicts high school math scores. J. Neurosci. 33 (1), 156–163. https://doi.org/10.1523/JNEUROSCI.2936-12.2013.
Rabe-Hesketh, S., Skrondal, A., Pickles, A., 2004. Generalized multilevel structural equation modeling. Psychometrika 69 (2), 167–190. https://doi.org/10.1007/BF02295939.
Reise, S.P., 2012. Invited paper: the rediscovery of bifactor measurement models. Multivar. Behav. Res. 47 (5), 667–696. https://doi.org/10.1080/00273171.2012.715555.
Reise, S.P., Morizot, J., Hays, R.D., 2007. The role of the bifactor model in resolving dimensionality issues in health outcomes measures. Qual. Life Res. Int. J. Qual. Life Asp. Treat. Care Rehabil. 16 (Suppl. 1), 19–31. https://doi.org/10.1007/s11136-007-9183-7.
Rypma, B., D'Esposito, M., 1999. The roles of prefrontal brain regions in components of working memory: effects of memory load and individual differences. Proc. Natl. Acad. Sci. 96 (11), 6558–6563. https://doi.org/10.1073/pnas.96.11.6558.
Schlösser, R.G.M., Wagner, G., Sauer, H., 2006. Assessing the working memory network: studies with functional magnetic resonance imaging and structural equation modeling. Neuroscience 139 (1), 91–103. https://doi.org/10.1016/j.neuroscience.2005.06.037.
Smith, S.M., Fox, P.T., Miller, K.L., Glahn, D.C., Fox, P.M., Mackay, C.E., Beckmann, C.F., 2009. Correspondence of the brain's functional architecture during activation and rest. Proc. Natl. Acad. Sci. U. S. A. 106 (31), 13040–13045. https://doi.org/10.1073/pnas.0905267106.
Steiger, J.H., 2007. Understanding the limitations of global fit assessment in structural equation modeling. Pers. Individ. Differ. 42 (5), 893–898. https://doi.org/10.1016/j.paid.2006.09.017.
Stephan, K.E., Marshall, J.C., Friston, K.J., Rowe, J.B., Ritzl, A., Zilles, K., Fink, G.R., 2003. Lateralized cognitive processes and lateralized task control in the human brain. Sci. (New York, N.Y.) 301 (5631), 384–386. https://doi.org/10.1126/science.1086025.
Sternberg, S., 1969. The discovery of processing stages: extensions of Donders' method. Acta Psychol. 30, 276–315. https://doi.org/10.1016/0001-6918(69)90055-9.
Sturgeon, J.A., Zautra, A.J., Arewasikporn, A., 2014. A multilevel structural equation modeling analysis of vulnerabilities and resilience resources influencing affective adaptation to chronic pain. Pain® 155 (2), 292–298. https://doi.org/10.1016/j.pain.2013.10.007.
Sugawara, H.M., MacCallum, R.C., 1993. Effect of estimation method on incremental fit indexes for covariance structure models. Appl. Psychol. Meas. 17 (4), 365–377. https://doi.org/10.1177/014662169301700405.

Suk, H.-I., Wee, C.-Y., Lee, S.-W., Shen, D., 2016. State-space model with deep learning for functional dynamics estimation in resting-state fMRI. NeuroImage 129, 292–307. https://doi.org/10.1016/j.neuroimage.2016.01.005.

Todd, J.J., Marois, R., 2005. Posterior parietal cortex activity predicts individual differences in visual short-term memory capacity. Cogn., Affect. Behav. Neurosci. 5 (2), 144–155. https://doi.org/10.3758/CABN.5.2.144.

Toit, S. H. C. du, Toit, M. du, 2008. Multilevel structural equation modeling. In: de Leeuw, J., Meijer, E. (Eds.), Handbook of Multilevel Analysis. Springer New York, pp. 435–478. https://doi.org/10.1007/978-0-387-73186-5_12.

Van Essen, D.C., Smith, S.M., Barch, D.M., Behrens, T.E.J., Yacoub, E., Ugurbil, K., 2013. The WU-Minn human connectome Project: an overview. NeuroImage 80, 62–79. https://doi.org/10.1016/j.neuroimage.2013.05.041.

Vossel, S., Weidner, R., Moos, K., Fink, G.R., 2016. Individual attentional selection capacities are reflected in interhemispheric connectivity of the parietal cortex. NeuroImage 129, 148–158. https://doi.org/10.1016/j.neuroimage.2016.01.054.

Vul, E., Harris, C., Winkielman, P., Pashler, H., 2009. Puzzlingly high correlations in fMRI studies of emotion, personality, and social cognition. Perspect. Psychol. Sci. 4 (3), 274–290. https://doi.org/10.1111/j.1745-6924.2009.01125.x.

Wang, K., Liang, M., Wang, L., Tian, L., Zhang, X., Li, K., Jiang, T., 2007. Altered functional connectivity in early Alzheimer's disease: a resting-state fMRI study. Hum. Brain Mapp. 28 (10), 967–978. https://doi.org/10.1002/hbm.20324.

Xia, M., Wang, J., He, Y., 2013. BrainNet viewer: a network visualization tool for human brain connectomics. PLoS One 8 (7), e68910. https://doi.org/10.1371/journal.pone.0068910.

Yarkoni, T., 2009. Big Correlations in Little Studies: inflated fMRI Correlations Reflect Low Statistical Power—commentary on Vul et al. (2009). Perspect. Psychol. Sci. 4 (3), 294–298. https://doi.org/10.1111/j.1745-6924.2009.01127.x.

Yarkoni, T., Braver, T.S., 2010. Cognitive neuroscience approaches to individual differences in working memory and executive control: conceptual and methodological issues. In: Gruszka, A., Matthews, G., Szymura, B. (Eds.), Handbook of Individual Differences in Cognition. Springer New York, pp. 87–107. https://doi.org/10.1007/978-1-4419-1210-7_6.

Yeo, B.T.T., Krienen, F.M., Sepulcre, J., Sabuncu, M.R., Lashkari, D., Hollinshead, M., Buckner, R.L., 2011. The organization of the human cerebral cortex estimated by intrinsic functional connectivity. J. Neurophysiol. 106 (3), 1125–1165. https://doi.org/10.1152/jn.00338.2011.

Zanto, T.P., Gazzaley, A., 2013. Fronto-parietal network: flexible hub of cognitive control. Trends Cogn. Sci. 17 (12) https://doi.org/10.1016/j.tics.2013.10.001.

Zhuang, J., LaConte, S., Peltier, S., Zhang, K., Hu, X., 2005. Connectivity exploration with structural equation modeling: an fMRI study of bimanual motor coordination. NeuroImage 25 (2), 462–470. https://doi.org/10.1016/j.neuroimage.2004.11.007.